Clays and Clay Minerals, Vol. 68, No. 3:220–236, 2020

ADSORPTIVE REMOVAL OF Ni^{2+} IONS FROM AQUEOUS SOLUTIONS BY NODULAR SEPIOLITE (MEERSCHAUM) AND INDUSTRIAL SEPIOLITE SAMPLES FROM ESKIŞEHIR, TURKEY

İLKER KIPÇAK*, EMEL KURTARAN ERSAL, AND MINE ÖZDEMIR

[1]Department of Chemical Engineering, Eskişehir Osmangazi University, 26480 Eskişehir, Turkey

Abstract—Heavy metals in the environment are a problem due to their toxicity and bioaccumulation. Adsorptive removal of heavy metals by clay minerals has garnered increasing attention due to the abundance, low cost, and exceptional physicochemical properties of the clays. The purpose of the present study was to investigate the utilization of two Turkish sepiolite samples, nodular sepiolite (NS) and industrial sepiolite (IS), as adsorbents in removing Ni^{2+} ions from aqueous solutions. The specific surface areas of NS and IS are 182.19 $m^2\ g^{-1}$ and 63.78 $m^2\ g^{-1}$, respectively. The effects of adsorbent dosage, initial pH, contact time, initial concentration, and temperature on the adsorption of Ni^{2+} ions onto the sepiolite samples were investigated using a batch method. The optimum adsorbent dosage was determined as 0.6 g/50 mL of adsorbent and the optimum pH value was 6.0, for both sepiolite samples. The adsorption process obeyed the Freundlich isotherm model (K_F: 4.89–9.73 $mg^{1-1/n}\ L^{1/n}\ g^{-1}$ for NS and 4.27–6.42 $mg^{1-1/n}\ L^{1/n}\ g^{-1}$ for IS) and the pseudo-second order kinetics model (k_2: 0.0049–0.0397 g $mg^{-1}\ min^{-1}$ for NS and 0.0688–0.1195 g $mg^{-1}\ min^{-1}$ for IS). The adsorption process was spontaneous and endothermic, and the randomness increased. The samples exhibited large adsorption capacities through three cycles of adsorption-desorption tests. The results revealed that the sepiolite samples are promising as cost-effective adsorbents for the removal of Ni^{2+} ions from aqueous solutions.

Keywords—Adsorption · Isotherm · Kinetics · Ni removal · Sepiolite · Thermodynamics

INTRODUCTION

Sepiolite is a fibrous clay mineral comprising tetrahedral and octahedral oxide/hydroxide sheets. The chemical formula is $Mg_8Si_{12}O_{30}(OH)_4(H_2O)_4.8H_2O$. It has molecule-sized channels (0.37 nm×1.06 nm) oriented along the longitudinal direction of the fiber (Brauner and Preisinger 1956). A microscopic and sometimes macroscopic level of fibrous morphology differentiates the mineral from laminar clay minerals. Its fibrous morphology, small particle size, and intra-crystalline channels result in large specific surface areas. The BET specific surface area for sepiolite was reported to be in the range ~80 to 350 $m^2\ g^{-1}$ (Suarez and Garcia-Romero 2012). Such a large BET surface area allows sepiolite to adsorb ions, polar liquids, water, and also molecules such as drugs or insecticides. Oxygen atoms in the tetrahedral sheet, water molecules coordinated with Mg^{2+} ions at the edge of the structure, and silanol groups resulting from the breakdown of Si–O–Si bonds are active adsorption centers on the sepiolite surface and provide a large adsorption capacity to the mineral (Yebra-Rodriguez et al. 2003).

Sepiolite may appear in two forms: α-sepiolite which occurs as large bundles of crystalline fibers, and β-sepiolite which occurs as amorphous aggregates or small flat rounded particles (Fersman 1913). Nodular sepiolite (meerschaum) is a well known clay that has been exploited in Eskişehir province (Turkey) for centuries. It is a soft white clay mineral often used to make souvenirs such as tobacco pipes (known as meerschaum pipes) by carving. The carving residues, which occur in large amounts, have not found a profitable use to date. Several layered sepiolite occurrences have been discovered in Neogene lacustrine sediments near Eskişehir. Of these, four layered sepiolite occurrences are mined currently around Eskişehir, and low-grade sepiolite clays are exploited for the production of cat litter (Yeniyol 2014).

Heavy metals are defined generally as metallic chemical elements the atomic weights of which are between 63.5 and 200.6 and also have a specific gravity of >5.0 (Srivastava and Majumder 2008). They are natural components of the Earth's crust and can enter a water source through industrial or consumer waste, or even by acid rain that dissolves and transports them to streams, rivers, lakes, and groundwater (Raval et al. 2016). Heavy metals are known to be toxic for aquatic organisms even at very low concentrations (Malkoç and Nuhoğlu 2006). Nickel (Ni) is a naturally occurring element found in all kinds of soils, and it is the world's 24th most abundant element comprising ~3% of the Earth's composition. It is a transition metal and can exist in several different oxidation states. The most common oxidation state of Ni is 2+ under normal environmental conditions (Cempel and Nikel 2006). Ni is used extensively in the production of alloys, coatings, batteries, and many other industrial products and, thus, significant amounts of it can find their way into the aquatic environment. According to the WHO (World Health Organization), the maximum acceptable concentration recommended for Ni in drinking water is 0.07 mg L^{-1} (WHO 2011). Because of its health hazards, numerous chemical and physical methods have been used to remove Ni from water and wastewater, including membrane filtration, coagulation or flocculation, flotation, electrochemical reduction/oxidation, precipitation, and ion exchange. Some limitations on these traditional

* E-mail address of corresponding author: ikipcak@ogu.edu.tr
DOI: 10.1007/s42860-020-00077-7

methods include poor removal efficiency, large operating cost, sensitive operating conditions, and secondary sludge production. Adsorption to clay minerals has advantages over the other methods, such as the small investment of initial capital and land required, the simplicity of design and operation, efficiency, large-scale applicability, and the fact that it is environmentally friendly (Raval et al. 2016). Among the other methods, clay minerals are used widely as adsorbents because of their low cost, large specific surface area, abundance, excellent adsorption properties, and non-toxic nature (Crini and Badot 2010). Recently, various clay minerals such as montmorillonite (Lin et al. 2017), bentonite (Glatstein and Francisca 2015), kaolinite (Zhao and He 2014), clinoptilolite (Milicevic et al. 2013), attapulgite (Guo et al. 2014), palygorskite (Sheikhhosseini et al. 2014), and sepiolite (Kocaoba 2009) were used widely even in their natural or modified forms for the removal of heavy metals from aqueous solutions. Among the clay minerals studied, sepiolite has attracted most attention especially for the removal of cadmium (Cd^{2+}), lead (Pb^{2+}), copper (Cu^{2+}), arsenic (As^{5+}), nickel (Ni^{2+}), iron (Fe^{2+}, Fe^{3+}), chromium (Cr^{3+}), manganese (Mn^{2+}), zinc (Zn^{2+}), strontium (Sr^{2+}), and antimony (Sb^{3+}) (Lazarevic et al. 2007; Kocaoba 2009; Guerra et al. 2010; Bahabadi et al. 2017; Dabiri and Shiraz 2018; Alvani et al. 2019; Kocaoba 2020). Although the results of metal removal by clay minerals are important and promising, most of these adsorbents suffer from limitations such as low removal efficiency, low stability, low mechanical strength, and non-durability. These restrictions have led to research for more efficient and cost-effective adsorbents.

The present study was undertaken to explore the feasibility of using nodular and industrial sepiolite samples from the Eskişehir region for the removal of Ni^{2+} ions from aqueous solutions by adsorption under various experimental conditions. To the authors' knowledge, no previous study has explored the performance of these sepiolite samples in Ni^{2+} removal. With this aim in mind, the effects of various parameters such as adsorbent dosage, initial pH, contact time, initial solution concentration, and temperature on the adsorption of Ni^{2+} ions were studied. Further aims were to apply pseudo-first order, pseudo-second order, and intraparticle diffusion kinetics models, to test the goodness of fit of Langmuir and Freundlich adsorption isotherms at various temperatures, and to test the spontaneity of such reactions by determining the thermodynamic parameters, then to estimate cost effectiveness.

MATERIALS AND METHODS

Materials

Two sepiolite samples were used in the experiments. One was nodular sepiolite as carving residue supplied by a workshop and having originally been excavated from the Türkmentokat-Gökçeoğlu region in Eskişehir. The other was an industrial sepiolite sample supplied by Sakarya Minerals Ind. Trade Co. Ltd. in Eskişehir, an organization which uses sepiolite in the manufacture of cat litter and adsorbents. These materials were chosen as adsorbents because of their low costs. The samples were coded as NS (nodular sepiolite) and IS (industrial sepiolite). They were ground and sieved to <75 μm (200 mesh) and dried at 100°C for 3 h. They were then stored in polypropylene bottles until needed for experiments and analyses.

A stock solution of 1000 mg Ni^{2+} L^{-1} was prepared from analytical-grade $NiCl_2.6H_2O$ obtained from Merck (Darmstadt, Germany). Solutions with concentrations required for adsorption experiments were prepared by diluting this stock solution with distilled water. The pH values of the solutions were adjusted using dilute NaOH (Merck, Darmstadt, Germany) and HCl (Riedel-de Haen, Seelze, Germany) solutions. The pH values of the solutions were measured using an HI 8314 model pH meter (Hanna, Póvoa de Varzim, Portugal).

Characterization Methods

X-ray diffraction (XRD) patterns of sepiolite samples were obtained by means of a Rint 2000 diffractometer (Rigaku, Tokyo, Japan) using CuKα radiation. The chemical compositions were determined using a ZSX Primus X-Ray Fluorescence (XRF) spectrometer (Rigaku, Tokyo, Japan). Textural properties were determined from nitrogen adsorption data obtained at –196°C with an Autosorb-1C surface area analyzer (Quantachrome, Boynton Beach, Florida, USA) at a relative pressure of 1.0. Specific surface areas were obtained using the multiple-point BET method. The total pore volumes were estimated by converting the amount of nitrogen gas adsorbed at P/P_0 = 0.99 to the volume of liquid nitrogen at the experimental condition. The micropore volumes were determined by means of the Dubinin Radushkevic (DR) method (Gregg and Sing 1982). Scanning electron micrographs of the samples before and after adsorption were obtained using a Regulus 8230 field emission scanning electron microscope (FE-SEM) (Hitachi, Tokyo, Japan). The sample surfaces were also analyzed by energy dispersive X-ray spectroscopy (EDS). Fourier-transform infrared spectroscopy (FTIR) spectra were collected with a Spectrum Two (Perkin Elmer, Waltham, Massachusetts, USA) model FTIR spectrophotometer in the 400–4000 cm^{-1} range using KBr pellets.

Adsorption Studies

A specific amount of adsorbent was placed in a capped conical flask and 50 mL of Ni^{2+} solution was added to it. The suspension was shaken at 150 rpm in a temperature-controlled water bath (BM 402, Nüve, Ankara, Turkey) at constant temperature for a fixed time period. The adsorbent was separated from the solution by filtration after adsorption and the Ni^{2+} concentration retained in the solution was determined by means of an ICE 3300 model atomic absorption spectrophotometer (Thermo Scientific, Shanghai, China) at a wavelength of 232 nm. The percentage of Ni^{2+} removed was calculated using the following equation:

$$\text{Removal}\ (\%) = \frac{(C_0 - C_t)}{C_0} * 100 \qquad (1)$$

https://doi.org/10.1007/s42860-020-00077-7 Published online by Cambridge University Press

Table 1. Chemical compositions of NS and IS

Component (%, w/w)	SiO_2	MgO	CaO	Fe_2O_3	Al_2O_3	K_2O	Cr_2O_3	L.O.I.
NS	48.91	30.73	2.38	0.24	–	–	–	17.73
IS	8.83	30.43	14.18	0.47	0.78	0.09	0.06	45.16

where C_0 (mg L^{-1}) is the initial concentration of solution and C_t (mg L^{-1}) is the concentration at time t (min). The adsorption capacity (q_t) was calculated using:

$$q_t = \frac{(C_0 - C_t) * V}{m} \quad (2)$$

where q_t (mg g^{-1}) is the adsorbed mass of Ni per unit mass of adsorbent, V (L) is the treated solution volume, and m (g) is the adsorbent mass.

In order to investigate the effect of adsorbent dosage, 0.1–1.0 g of adsorbent was added to 50 mL of 50 mg L^{-1} Ni^{2+} solution with pH 6 at 25°C for 24 h. The effect of pH was investigated by varying its value in the range of 2–8 with other conditions set at: 0.6 g/50 mL adsorbent dosage, 24 h contact time, 50 mg L^{-1} initial concentration, and 25°C temperature. To determine when the adsorption reached equilibrium, the experiments were also repeated for various time intervals (15–2880 min) under the conditions of pH 6, adsorbent dosage of 0.6 g/50 mL, initial Ni^{2+} concentration of 50 mg L^{-1} at 25, 35, or 45°C. The adsorption isotherms of Ni^{2+} were obtained after an equilibration time of 24 h and an initial concentration of 50–500 mg L^{-1} at 25–45°C, pH 6.0 and an adsorbent dosage of 0.6 g/50 mL. All the adsorption experiments were carried out in duplicate.

The fitting of kinetics and isotherm models was evaluated by the coefficient of determination (R^2) and chi-square (χ^2) measures and these were calculated as follows:

$$R^2 = \frac{\sum_{i=1}^{n}\left(q_{exp} - \overline{q_{cal}}\right)^2}{\sum_{i=1}^{n}\left(q_{exp} - \overline{q_{cal}}\right)^2 + \sum_{i=1}^{n}\left(q_{exp} - q_{cal}\right)^2} \quad (3)$$

$$\chi^2 = \sum_{i=1}^{n}\frac{\left(q_{exp} - q_{cal}\right)^2}{q_{cal}} \quad (4)$$

where q_{exp} and q_{cal} (mg g^{-1}) are the experimental and calculated Ni^{2+} adsorption capacities, respectively, and n is the number of measurements. The greater R^2 values indicate the

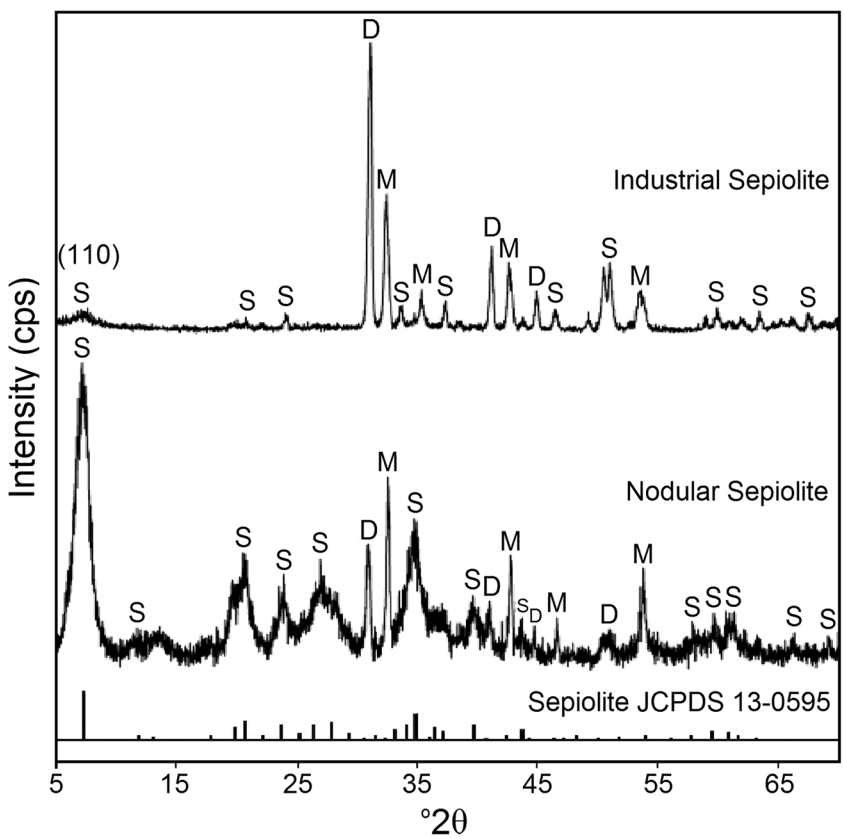

Fig. 1. XRD patterns of NS and IS (S: sepiolite, M: magnesite, D: dolomite)

https://doi.org/10.1007/s42860-020-00077-7 Published online by Cambridge University Press

Table 2. Textural properties deduced from N_2 adsorption at 77 K for NS and IS

Sample	S_{BET} ($m^2\ g^{-1}$)	V_{total} ($cm^3\ g^{-1}$)	V_{micro} ($cm^3\ g^{-1}$)	D_p (Å)
NS	182.19	0.2160	0.0054	47.59
IS	63.78	0.1278	0.0023	80.13

S: surface area; *V*: pore volume; D_p: pore diameter

appropriateness of the model fit. If the data calculated from the model were similar to those measured in the experiments, χ^2 would be small (Alvani et al. 2019).

Reusability of Adsorbent

Reusability tests were carried out in a similar way to adsorption studies. After adsorption experiments, Ni-loaded NS and IS samples were separated from the solution by filtration and then dried overnight for further use. For regeneration, the adsorbents used were treated with 25 mL of 0.1 M HCl solution at room temperature for 2 h and then washed with distilled water until neutral pH. The adsorption-desorption cycles were repeated three times by recording the Ni^{2+} adsorption capacities of adsorbents in each run. In addition, the Mg and Ca concentrations in the solutions after each regeneration effort were analyzed volumetrically by EDTA to determine the dissolution rates of the adsorbents (Gulensoy 1984).

RESULTS AND DISCUSSION

Characterization Results

The compositions of the NS and IS samples were determined by XRF analysis and are given in Table 1. The SiO_2 in the NS sample was a little lower and MgO was somewhat higher when compared with the chemical formula of sepiolite. In addition, the sample was determined to contain 2.38 wt.% CaO. These results were due to the sample containing magnesite ($MgCO_3$) and dolomite ($MgCa(CO_3)_2$) as impurities. Approximately 90% of NS by weight was sepiolite. The SiO_2 content of IS was quite low indicating that it was a low-grade sepiolite ore.

The XRD pattern of NS (Fig. 1) conformed to the standard pattern of sepiolite (JCPDS card No.13-0595). No impurities were identified except for small amounts of magnesite and dolomite indicating that the NS sample was a high-purity sepiolite. The sharp peaks in the XRD pattern of NS revealed the well crystallized character of the sample. The main reflection was observed in the 5–9°2θ region. This corresponds to an interlayer distance of about 12.43 Å. The XRD of the IS sample indicated the existence of plentiful dolomite (Fig. 1). The intensity of the 110 reflection, observed at 7.08°2θ, was that from which the interlayer distance was calculated to be 12.49 Å. The variations in d_{110} spacing of sepiolite have been studied by several researchers (Suarez and García-Romero 2012; Yeniyol 2014; Suarez et al. 2016). Sepiolite samples from the eastern part of Eskişehir were reported to appear together with other magnesic phyllosilicates and carbonates (dolomite and magnesite). Two distinct forms of sepiolite were distinguished in these samples: a well crystallized sepiolite with a 110 reflection at 12.07–12.3 Å, and a poorly crystallized sepiolite in which the 110 reflection occurs at 12.7–13.0 Å. In the XRD pattern of randomly oriented samples in which smectite predominates, the (001) basal reflection is weak and asymmetric and is centered at 12.5 Å (Yeniyol 2014).

The data in Table 2 indicate the surface areas, pore volumes, and average pore diameters for the NS and IS samples.

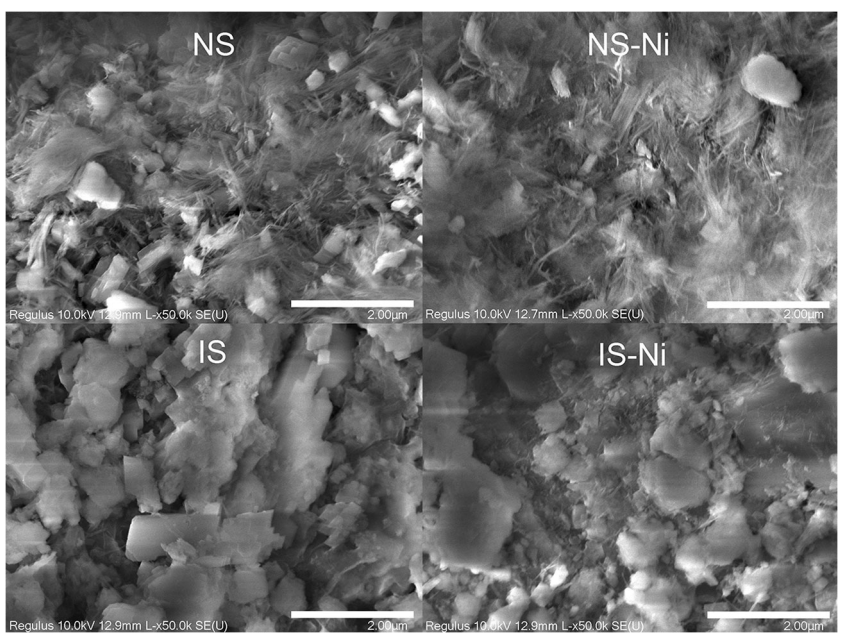

Fig. 2. SEM images of NS, IS, NS-Ni, and IS-Ni samples. Scale bars are 2.00 µm

https://doi.org/10.1007/s42860-020-00077-7 Published online by Cambridge University Press

The BET specific surface area of NS (182.19 $m^2 g^{-1}$) was three times larger than that of IS (63.78 $m^2 g^{-1}$). In addition, larger micro and total pore volumes of NS showed that the material had a more porous structure.

The morphologies of the NS and IS samples were also studied by SEM. As seen in Fig. 2, the morphologies of the two sepiolite samples are significantly different. The NS sample showed a more porous and fibrous morphology. Scattered acicular minerals and mineral aggregates were found on the surface of the sample. In contrast, in the photomicrograph of IS, a rough surface with irregular particles of micron and submicron size was observed and most of these particles were subhedral. Small amounts of fibrous particles were also observed on the surface of IS. The fibrous structure of NS continued to exist after the adsorption of Ni but its morphology had changed a little. The SEM images of the Ni-adsorbed IS sample (IS-Ni) indicate smaller particle size than the raw sample (IS). The surface was covered with micrometric particles.

Analysis by energy dispersive X-ray spectroscopy (EDS) showed that the NS consisted of Mg, Si, O, and C while the IS consisted of Mg, Si, O, C, Ca, and Al (Fig. 3). The EDS spectra of the NS-Ni and IS-Ni samples illustrated the existence of Ni in the samples, thus proving the adsorption. 3.72% and 2.90% of Ni were detected on NS-Ni and IS-Ni, respectively.

The various functional groups in the sepiolite samples (NS and IS) and also in the Ni-loaded samples (NS-Ni and IS-Ni) were measured with FTIR (Fig. 4, Table 3). The IR bands at 3690 cm^{-1} for NS and 3687 cm^{-1} for IS were assigned to the surface Mg–OH stretching vibration (Eren and Gumus 2011; Frost et al. 2001). The bands at 3572 cm^{-1} for NS and 3564 cm^{-1} for IS were related to the stretching modes of water molecules coordinated with Mg ions. The 3421 cm^{-1} and 3397 cm^{-1} bands for NS and IS, respectively, were attributed to zeolitic water and the band at 3261 cm^{-1} for NS was assigned to the coordinated water (Frost et al. 2001; Lazarevic et al. 2010; Franco et al. 2014). The bands at 2932 and 2904 cm^{-1} were attributed to the C–H stretching vibrations (Alkan et al. 2005). The presence of dolomite and magnesite impurities was confirmed by the bands at 2532, 1452, 884, and 728 cm^{-1} for NS and by the bands at 2531, 1822, 1448, 885, and 730 cm^{-1} for IS (Lescano et al. 2014; Kıpçak and Isıyel 2015; Sabah and Ouki 2017; Wu et al. 2017). These bands proving the presence of carbonate are in agreement with the results of chemical analysis and XRD patterns given in Fig. 1. The band at 1659 cm^{-1} for NS was due to the –OH bending vibrations of zeolitic water (Qiu et al. 2013; Sabah and Ouki 2017). The bands in the 1250–400 cm^{-1} range were characteristic of the silicate structure of sepiolite. The bands observed at 1210, 1077, and 1016 cm^{-1} for NS and at 1212 and 1012 cm^{-1} for IS were produced by the Si–O vibrations (Eren et al. 2010; Ahribesh et al. 2017). The band observed at 784 cm^{-1} for NS was the O–H bending vibration of Mg–Fe–OH (Duman et al. 2015). The bands at 749 and 747 cm^{-1} for NS and IS, respectively, were assigned to the Si–O bonds (Xu et al. 2017).

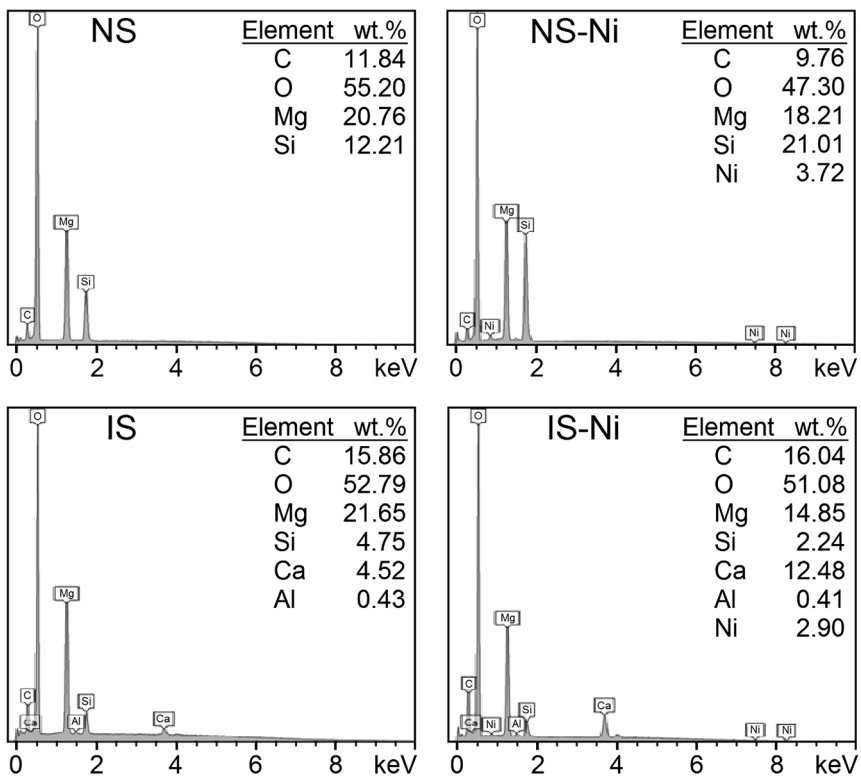

Fig. 3. EDS elemental analyses of NS, IS, NS-Ni, and IS-Ni samples

https://doi.org/10.1007/s42860-020-00077-7 Published online by Cambridge University Press

The band at 471 cm^{-1} observed in the spectrum of NS could be attributed to an O–Si–O bending (Lescano et al. 2014; Eren et al. 2010). The bands at 440 and 427 cm^{-1} originated from octahedral–tetrahedral bonds (Si–O–Mg bonds). The bands at 690 and 645 cm^{-1} for NS and at 690 and 655 cm^{-1} for IS corresponded to the Mg–OH bond vibrations (Lazarevic et al. 2010; Ahribesh et al. 2017).

Some slight shifts were observed in the IR absorption bands of the samples after Ni^{2+} adsorption (Fig. 4). For the NS sample, the shift in the –OH stretching band after Ni^{2+} adsorption from 3421 to 3424 cm^{-1} was attributed to the attachment of Ni^{2+} to the –OH groups. The shift of the band at 1659 to 1661 cm^{-1} and the weakening intensity of this band after adsorption indicated the decrease in the zeolitic water content with the replacement of the introduced Ni^{2+} ions. The shift of the 1210 cm^{-1} band to 1212 cm^{-1} confirmed the involvement of the Si–O bond linkage in the Ni^{2+} adsorption process. For the IS sample, the band of the triple bridge group Mg_3OH shifted from 3687 to 3684 cm^{-1}. The shift from 3397 to 3419 cm^{-1} in the absorption band of –OH stretching vibrations indicated clearly the involvement of the –OH group as active sites for binding of Ni^{2+} cations. The shift in the stretching vibration band of Si–O from 1212 to 1214 cm^{-1}; and the bending vibration band of Mg–OH from 690 to 685 cm^{-1} were also observed. These shifts in the absorption bands suggested that –OH and Si–O groups functioned as adsorption sites for Ni^{2+} ions from solution.

Effect of Adsorbent Dosage

Adsorbent dosage plays a major role in the adsorption process because it determines the capacity of an adsorbent for a given initial concentration of adsorbate. In order to investigate the effect of adsorbent dosage on the efficient removal of Ni^{2+}, batch experiments were carried out with 50 mg L^{-1} Ni^{2+} solution by varying the adsorbent dose from 0.1 to 1.0 g/50 mL. While the adsorbent dosage increased from 0.1 to 0.6 g/50 mL, the removal percentages of Ni^{2+} ions for NS and IS samples increased from 36.68 to 97.61% and from 36.70 to 99.07%, respectively (Fig. 5). Further increases in the adsorbent dosage up to 1.0 g/50 mL failed to cause any significant change in the removal yields. This behavior may be explained by the increased surface area and effective adsorption sites on the adsorbent surface with increasing adsorbent dosage (Uddin 2017). The optimum adsorbent dosage was chosen, therefore, as being 0.6 g/50 mL for both adsorbents.

Effect of Initial pH

The pH of the solution is one of the parameters that has a significant effect on the adsorption of metal ions because the

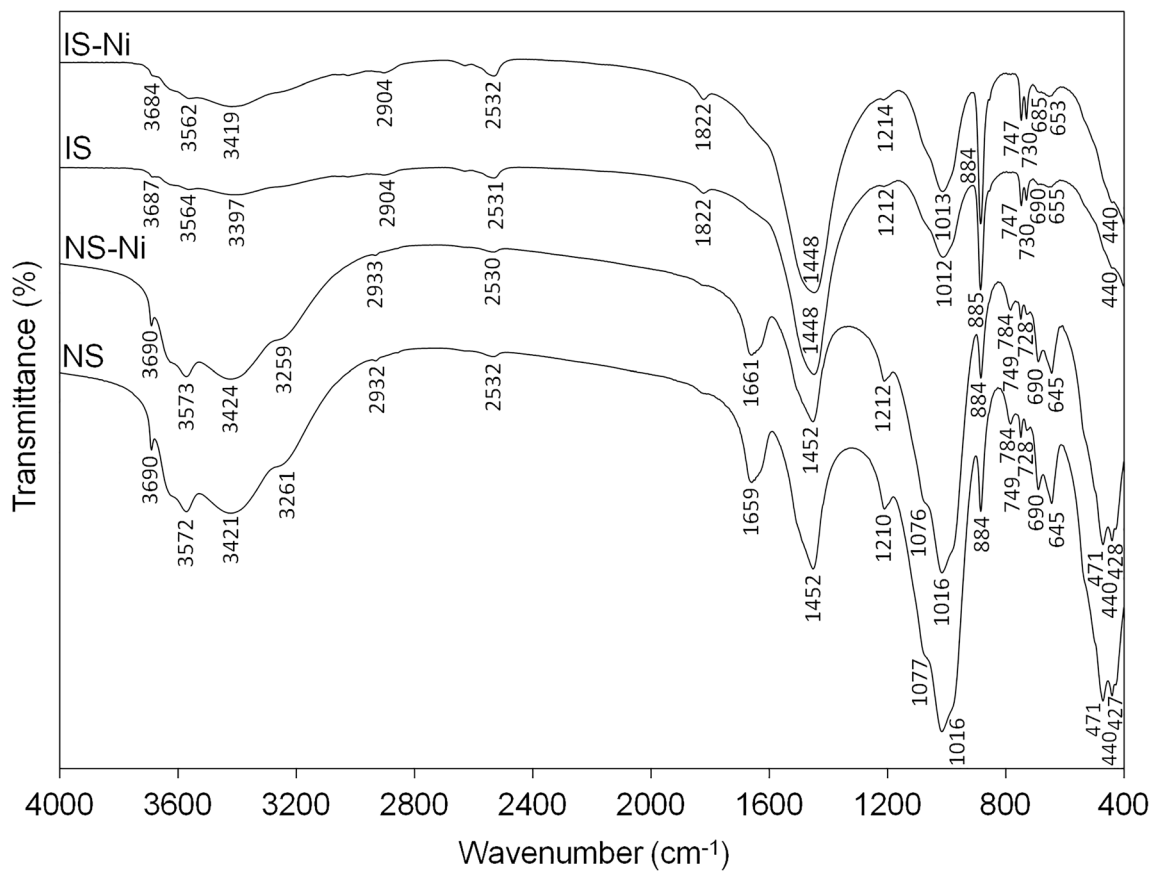

Fig. 4. FTIR spectra of NS, IS, NS-Ni, and IS-Ni samples

https://doi.org/10.1007/s42860-020-00077-7 Published online by Cambridge University Press

Table 3. Functional groups in NS, NS-Ni, IS, and IS-Ni samples

Functional group	Wavenumber (cm^{-1})			
	NS	NS-Ni	IS	IS-Ni
Mg–OH stretching	3690	3690	3687	3684
–OH stretching	3572–3421–3261	3573–3424–3259	3564–3397	3562–3419
C–H stretching	2932	2933	2904	2904
Carbonate impurity	2532	2530	2531–1822	2532–1822
–OH bending	1659	1661	–	–
Carbonate impurity	1452	1452	1448	1448
Si–O stretching	1210–1077–1016	1212–1076–1016	1212–1012	1214–1013
Carbonate impurity	884	884	885	885
–OH bending	784	784	–	–
Si–O vibration	749	749	747	747
Carbonate impurity	728	728	730	730
Mg–OH bending	690–645	690–645	690–655	685–653
O–Si–O bending	471	471	–	–
Si–O–Mg vibration	440–427	440–428	440	440

surface charge density of the adsorbent and the metal speciation depend on the pH. The change of pH affected significantly the morphology of Ni species in the solution, which further affected the adsorption process of this metal. The main species of Ni was Ni^{2+} when the pH of the solution was <7.0. When the pH was >7.0, $Ni(OH)_2$ occurred and its proportion apparently increased with increasing pH (Sheikhhosseini et al. 2014; An et al. 2019). The effect of pH was studied at various pH values ranging from 2 to 8 (Fig. 6). Ni^{2+} adsorption capacities of both adsorbents increased with increasing pH until 4, and then stayed almost constant. This situation is related to the active sites on the adsorbents. At lower pH values, the concentration of H^+ ions is high, causing competition between the proton and metal ions for vacant adsorbent sites. The removal efficiency, therefore, is less at lower pH values. Furthermore, when the active sites are protonated, the surface is positively charged and the adsorption of metal ions on the surface is reduced. The final pH values of the solutions after the pH experiments were checked and found to be <7 (for initial pH ≤7) or just above 7 (for initial pH = 8). This meant that the main species of Ni in the solutions were Ni^{2+} ions. Mg–OH and Si–OH groups on the sepiolite (S) surface were reported to play important roles in metal ion adsorption. S–O–Ni^+ and $(S–O)_2$–Ni complexes might be formed in the interactions between Ni^{2+} ions and the S–OH surface functional groups (Lazarevic et al. 2007). In addition, the clay surface may also

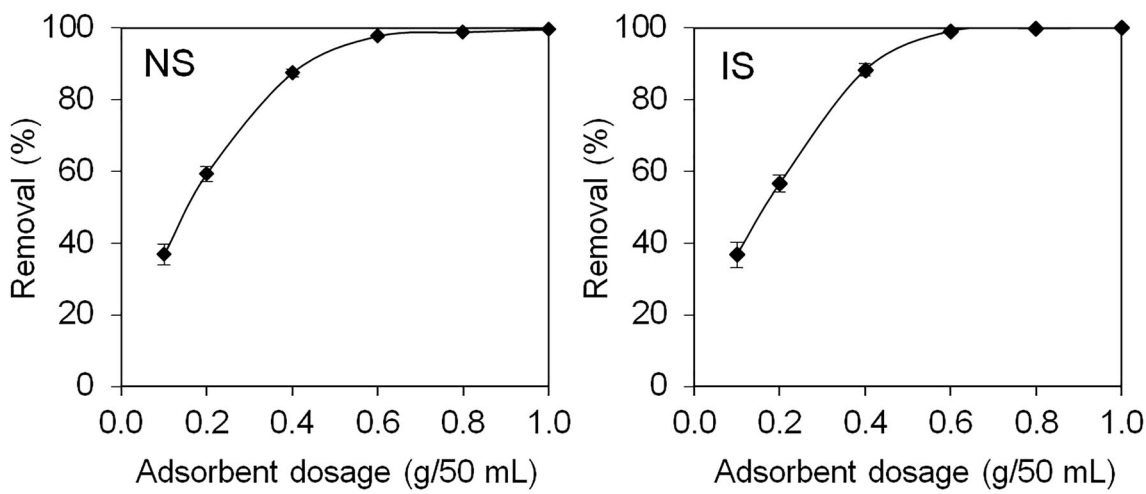

Fig. 5. Effect of adsorbent dosage on the removal of Ni^{2+} ions by NS and IS (pH: 6.0, *t*: 24 h, C_0: 50 mg L^{-1}, *T*: 25°C). The error bars represent the standard deviation

https://doi.org/10.1007/s42860-020-00077-7 Published online by Cambridge University Press

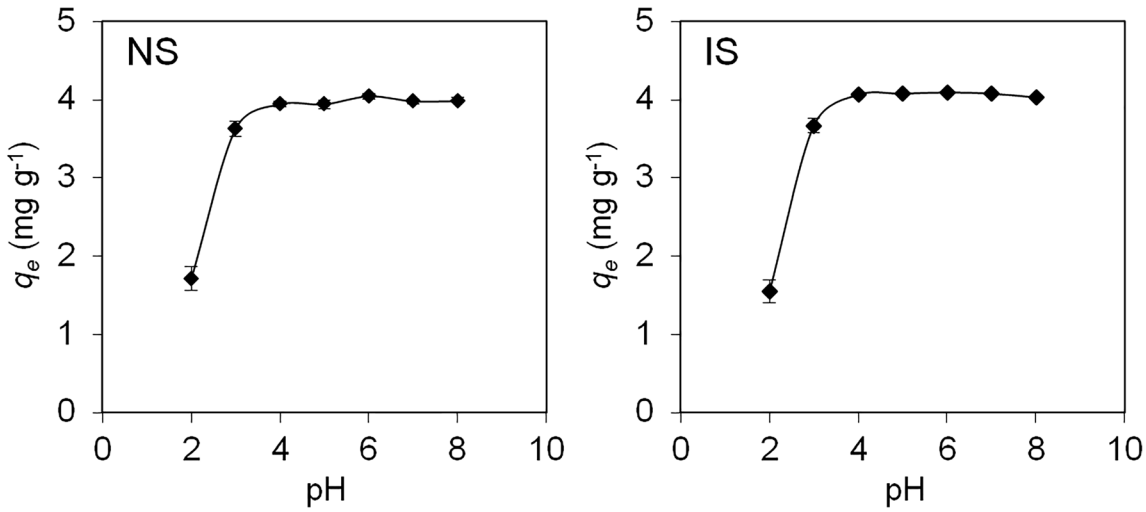

Fig. 6. Effect of initial pH on the adsorption of Ni^{2+} ions by NS and IS (adsorbent dosage: 0.6 g/50 mL, *t*: 24 h, C_0: 50 mg L^{-1}, *T*: 25°C). The error bars represent the standard deviation

be negatively charged providing adsorption sites for metal cations. Accordingly, the Si–O^- groups formed by the break-up of Si–O–Si bonds might be complexed as $(Si–O)_2$–Ni (Yavuz et al. 2003). The original pH value of the Ni^{2+} solution was 6; therefore, this value was chosen as the optimum pH value and applied throughout all of the adsorption experiments. In addition, Ni precipitation was reported to be negligible at pH 6 (Carvalho et al. 2008).

Effect of Contact Time

The time required to achieve equilibrium for the metal ions and adsorbent is very important in the adsorption experiment because it depends on the nature of the system used. The effect of contact time on the adsorption of Ni^{2+} ions was investigated between 15 and 2880 min time intervals at 25, 35, and 45°C (Fig. 7). During short contact times, adsorption was very fast (within 15 min, >50% was adsorbed) due to the presence of numerous active sites on the adsorbent surface. The adsorption rate then decreased because of the decrease in the number of adsorption sites and in the Ni^{2+} concentration gradient. The equilibrium was almost reached in 960 min for NS and 720 min for IS. However, experiments were carried out with 24 h of contact time to achieve equilibrium at the solid/liquid interface and to ensure the best adsorption conditions at higher concentrations (Guerra et al. 2010).

Effect of Initial Concentration

The effect of initial concentration on the amount of Ni^{2+} ions adsorbed was studied with varying initial concentrations (50–500 mg L^{-1}) at three different temperatures of 25, 35, and

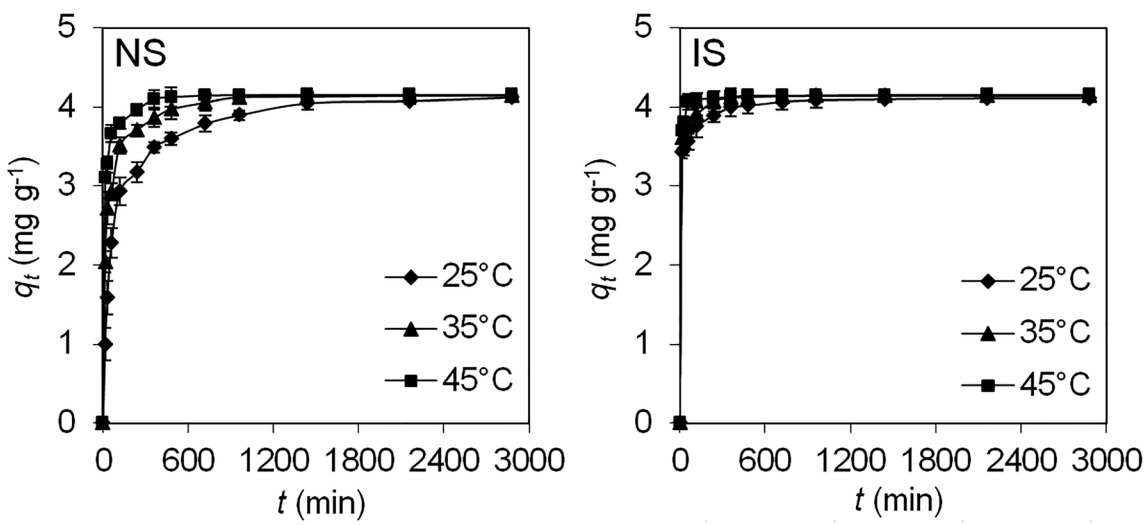

Fig. 7. Effect of contact time on the adsorption of Ni^{2+} ions by NS and IS at three temperatures (adsorbent dosage: 0.6 g/50 mL, pH: 6, C_0: 50 mg L^{-1}). The error bars represent the standard deviation

https://doi.org/10.1007/s42860-020-00077-7 Published online by Cambridge University Press

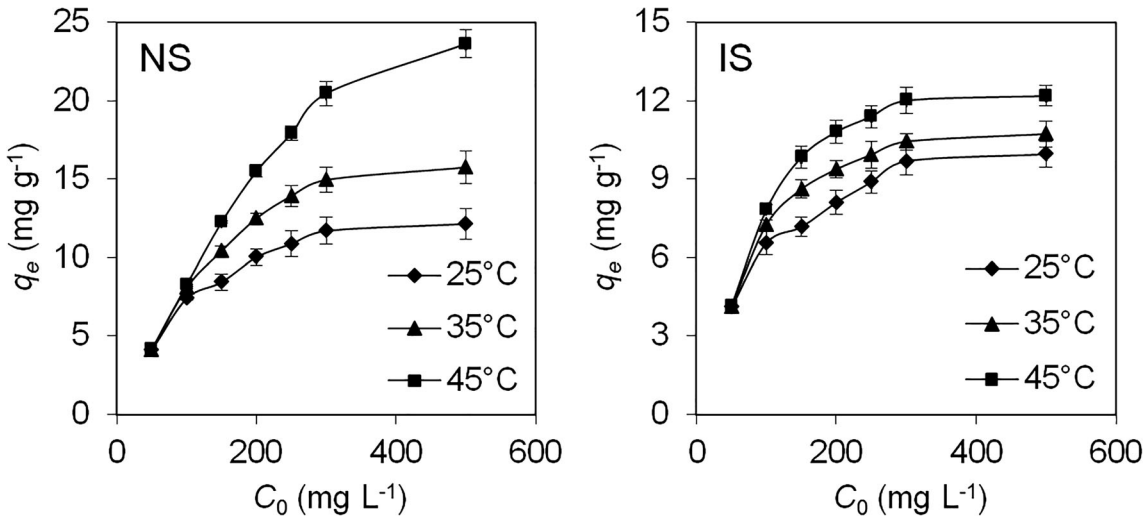

Fig. 8. Effect of initial concentration on the adsorption of Ni^{2+} ions by NS and IS at three temperatures (adsorbent dosage: 0.6 g/50 mL, pH: 6, *t*: 24 h). The error bars represent the standard deviation

45°C. According to the results (Fig. 8), the adsorption capacities of both sepiolites increased with increasing initial Ni^{2+} concentration. This result showed that the initial concentration of Ni^{2+} provided a driving force to overcome the mass transfer resistances between the adsorption medium and adsorbent. With more Ni^{2+} in solution, more active sites of the sepiolites were involved in the adsorption process. Larger ion concentrations enhanced the mass transfer driving force, and increased the equilibrium uptake capacity of metal ions. The adsorption capacity increased also with increasing temperature, indicating that the reaction follows the endothermic pathway. The increase in the adsorption capacity with temperature may be due to various factors such as increase in the interreaction between adsorbent and adsorbate, formation of new adsorption sites, and an increasing rate of intraparticle diffusion at higher temperatures.

Adsorption Kinetics

In order to investigate the controlling mechanism of the adsorption processes, pseudo-first order, pseudo-second order, and intraparticle diffusion kinetics models were applied to the experimental data. The pseudo-first order model was first developed by Lagergren (1898). The differential form of the model is described by Eq. 5 (Lagergren 1898):

$$\frac{dq_t}{dt} = k_1(q_e - q_t) \quad (5)$$

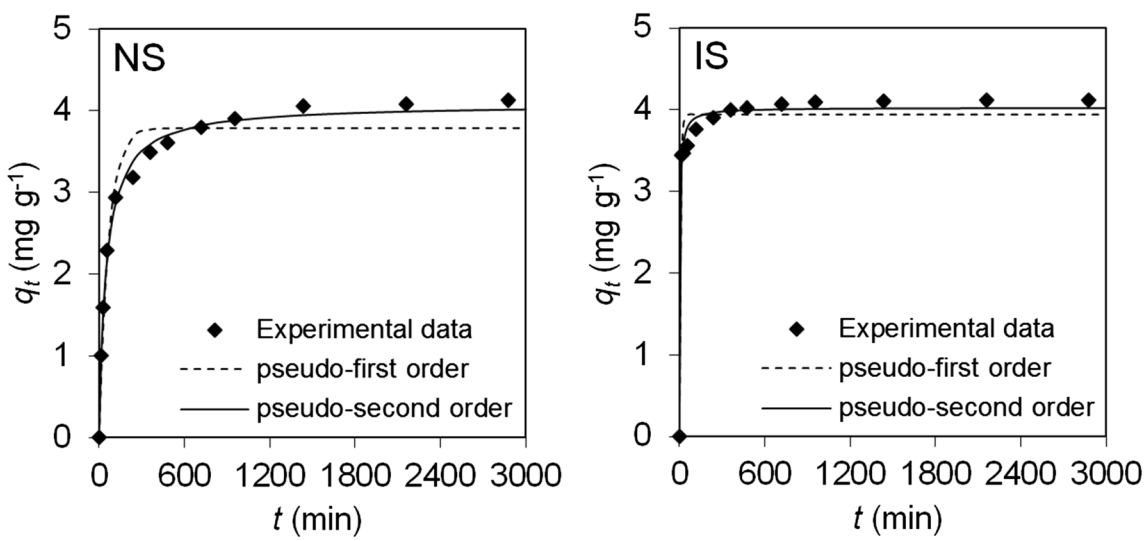

Fig. 9. Pseudo-first order and pseudo-second order kinetics plots for the adsorption of Ni^{2+} ions by NS and IS at 25°C

https://doi.org/10.1007/s42860-020-00077-7 Published online by Cambridge University Press

Table 4. Kinetics parameters for the adsorption of Ni^{2+} ions by NS and IS at three temperatures

	NS			IS		
	25°C	35°C	45°C	25°C	35°C	45°C
q_{exp} (mg g^{-1})	4.05	4.13	4.15	4.09	4.14	4.15
Pseudo-first order						
q_e (mg g^{-1})	3.79	3.94	4.02	3.94	4.04	4.11
k_1, 10^{-2} (min^{-1})	1.49	3.64	8.12	12.16	13.69	14.48
R^2	0.964	0.953	0.969	0.970	0.983	0.995
χ^2	0.300	0.280	0.135	0.119	0.065	0.020
Pseudo-second order						
q_e (mg g^{-1})	4.08	4.11	4.13	4.03	4.11	4.15
k_2, 10^{-2} (g mg^{-1} min^{-1})	0.49	1.40	3.97	6.88	8.97	11.95
R^2	0.995	0.992	0.994	0.989	0.995	0.999
χ^2	0.032	0.048	0.028	0.046	0.020	0.003
Intraparticle diffusion						
k_p, 10^{-2} (mg g^{-1} $min^{-1/2}$)	5.32	3.34	1.71	1.35	0.96	0.60
C	1.92	2.83	3.50	3.57	3.77	3.92
R^2	0.772	0.725	0.699	0.776	0.710	0.632
χ^2	1.309	0.597	0.171	0.056	0.047	0.037

where q_e and q_t (mg g^{-1}) are the amounts of metal ions adsorbed per gram of adsorbent at equilibrium and at any time t (min), respectively, and k_1 (min^{-1}) is the rate constant of pseudo-first order adsorption. By integrating the equation with the suitable boundary condition (i.e. $q_0 = 0$), the expression becomes:

$$q_t = q_e\left(1-e^{-k_1 t}\right) \quad (6)$$

The differential form of the pseudo-second order kinetics rate equation is expressed as (Ho and McKay 1998):

$$\frac{dq_t}{dt} = k_2(q_e - q_t)^2 \quad (7)$$

where k_2 (g mg^{-1} min^{-1}) is the rate constant of pseudo-second order adsorption. The integrated form is:

$$q_t = \frac{k_2 q_e^2 t}{1 + k_2 q_e t} \quad (8)$$

The nonlinear plots for the pseudo-first order and pseudo-second order kinetics models for the adsorption of Ni^{2+} by NS

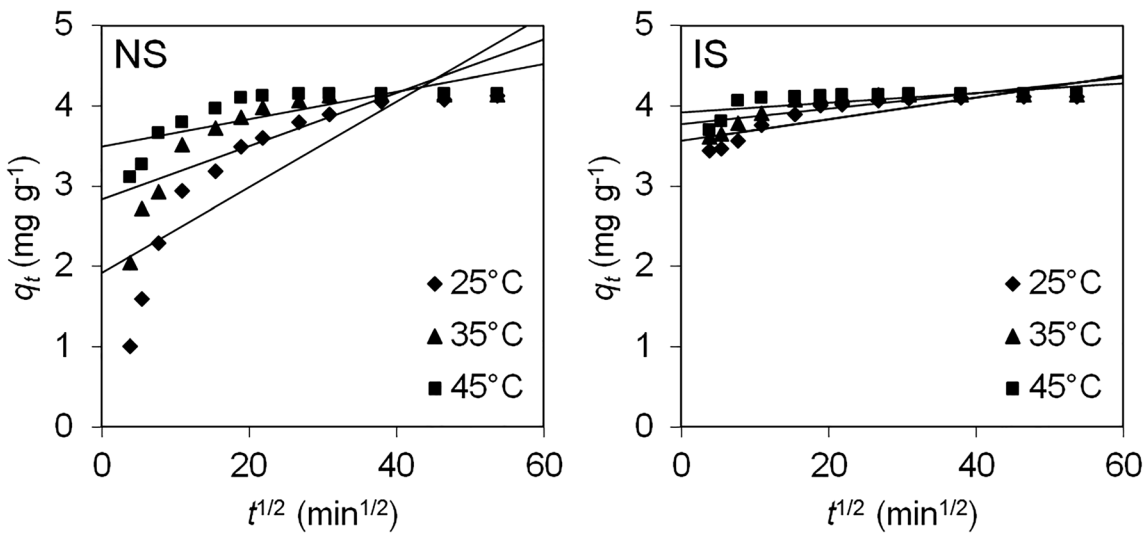

Fig. 10. Intraparticle diffusion plots for the adsorption of Ni^{2+} ions by NS and IS at three temperatures

https://doi.org/10.1007/s42860-020-00077-7 Published online by Cambridge University Press

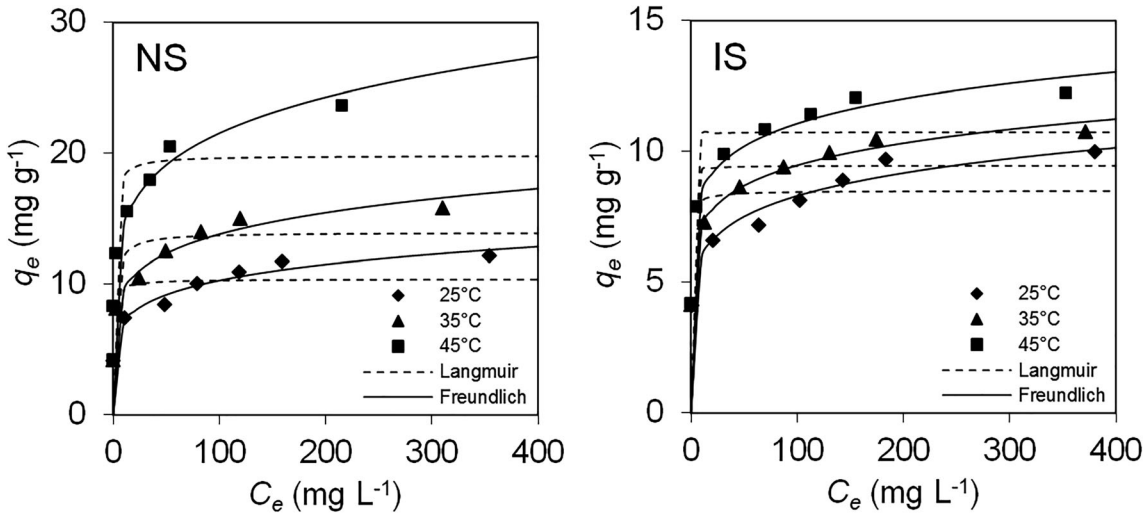

Fig. 11. Langmuir and Freundlich isotherm plots for the adsorption of Ni^{2+} ions by NS and IS at three temperatures

and IS at 25°C (Fig. 9) were processed using nonlinear optimization techniques to yield the parameters k_1, k_2, and q_e (Table 4). The intraparticle diffusion model is described by the following equation (Weber and Morris 1963):

$$q_t = k_p t^{1/2} + C \quad (9)$$

where k_p (mg g^{-1} min$^{-1/2}$) is the intraparticle diffusion rate constant and C is the experiment constant. By plotting q_t vs $t^{1/2}$ (Fig. 10), the rate constant is obtained from the slope and C from the intercept. The plot of q_t vs $t^{1/2}$ should be linear if intraparticle diffusion is involved in the adsorption process, and becomes the rate-controlling step if this line passes through the origin. When the plot does not pass through the origin, this is an indication of some degree of boundary layer control and shows that intraparticle diffusion is not the only process affecting the rate.

The determination coefficients (R^2) for the pseudo-second order kinetics model are larger than those for pseudo-first order and intraparticle diffusion models, indicating that the pseudo-second order model is more suitable for describing the adsorption behavior of Ni^{2+} onto the NS and IS (Table 4). Besides, the q_e values calculated by the pseudo-second order model were closer to the experimental q_{exp} than pseudo-first order, suggesting that the curve modeled by the pseudo-second order equation is more consistent with the experimental data. The increase in rate constants (k_2) with increasing temperature indicated the endothermic nature of adsorption.

Adsorption Isotherms

Adsorption isotherms are used to study the equilibrium distribution of metal ions between solid adsorbent and liquid phase. The two best known isotherm models are the Langmuir and the Freundlich. The non-linear form of the Langmuir equation, which is valid for monolayer adsorption onto a

Table 5. Langmuir and Freundlich constants for the adsorption of Ni^{2+} ions by NS and IS at three temperatures

	NS			IS		
	25°C	35°C	45°C	25°C	35°C	45°C
q_{exp} (mg g^{-1})	12.15	15.76	23.63	9.96	10.73	12.19
Langmuir						
q_m (mg g^{-1})	10.37	13.94	19.81	8.49	9.45	10.73
K_L (L mg^{-1})	1.16	0.60	1.05	1.72	4.83	12.97
R^2	0.774	0.827	0.859	0.747	0.806	0.799
χ^2	1.516	8.488	13.993	1.016	0.826	1.185
Freundlich						
K_F (mg$^{1-1/n}$ L$^{1/n}$ g^{-1})	4.89	6.55	9.73	4.27	5.36	6.42
n	6.19	6.17	5.79	6.92	8.09	8.46
R^2	0.974	0.975	0.981	0.965	0.991	0.985
χ^2	0.126	0.265	0.601	0.117	0.030	0.076

https://doi.org/10.1007/s42860-020-00077-7 Published online by Cambridge University Press

Table 6. Comparison of the adsorption abilities of various adsorbents for Ni

Adsorbent type	Max. adsorption capacity (mg g^{-1})	T (°C)	pH	References
Activated carbon	63.74	22	6.0	Pap et al. (2017)
Activated carbon	17.24	23	5.0	Lata et al. (2008)
Modified biochar	38.97	23	6.0	Mahdi et al. (2019)
Modified pine bark	20.58	20	8.0	Argun et al. (2005)
Biosorbent (*Saccharum bengalense*)	15.79	60	5.0	Din and Mirza (2013)
Waste tea	15.26	25	4.0	Malkoç and Nuhoğlu (2005)
Lignite	13.00	20	4.5	Pehlivan and Arslan (2007)
Sludge-derived MnO_2	119.76	25	6.5	Ong et al. (2018)
Magnetite based nanocomposite	20.53	20	8.0	Baseri and Tizro (2017)
Montmorillonite	21.14	30	5.7	Gupta and Bhattacharyya (2006)
Vermiculite	25.51	25	6.0	Katsou et al. (2010)
Bentonite	19.92	25	6.0	Katsou et al. (2010)
Zeolite	16.86	25	6.0	Katsou et al. (2010)
Modified montmorillonite	4.73	25	6.0	Carvalho et al. (2008)
Iranian sepiolite	4.81	25	7.3	Sheikhhosseini et al. (2014)
Palygorskite	2.41	25	6.9	Sheikhhosseini et al. (2014)
Kaolinite	1.67	25	–	Yavuz et al. (2003)
Volcanic rock pumice	1.19	25	5.0	Alemayehu and Lennartz (2010)
Volcanic rock scoria	0.98	25	5.0	Alemayehu and Lennartz (2010)
Nodular sepiolite (NS)	12.15	25	6.0	Present study
Industrial sepiolite (IS)	9.96	25	6.0	Present study

homogeneous surface with a finite number of identical sites, is (Langmuir 1918):

$$q_e = \frac{q_m K_L C_e}{1 + K_L C_e} \quad (10)$$

where C_e (mg L^{-1}) is the equilibrium metal ion concentration, q_e (mg g^{-1}) is the amount of metal ion adsorbed per unit weight of adsorbent at equilibrium, K_L (L mg^{-1}) is the Langmuir constant related to the enthalpy of adsorption, and q_m (mg g^{-1}) is the maximum adsorption capacity.

The Freundlich adsorption isotherm has been interpreted as adsorption to heterogeneous surfaces sites. The non-linear Freundlich equation is (Freundlich 1926):

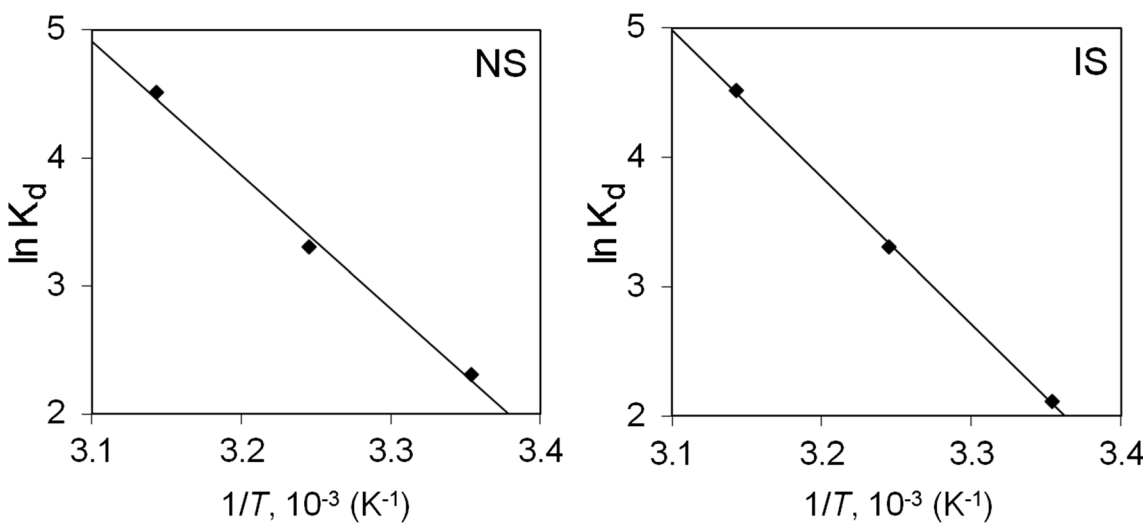

Fig. 12. Plots of ln K_d vs $1/T$ for estimation of thermodynamic state functions

https://doi.org/10.1007/s42860-020-00077-7 Published online by Cambridge University Press

Table 7. Thermodynamic state functions for the adsorption of Ni^{2+} ions by NS and IS

Adsorbent type	$\Delta H°$ (kJ mol^{-1})	$\Delta S°$ (J mol^{-1} K^{-1})	$\Delta G°$ (kJ mol^{-1})		
			25°C	35°C	45°C
NS	86.77	309.81	–5.70	–8.46	–11.92
IS	94.51	334.41	–5.24	–8.47	–11.93

$$q_e = K_F C_e^{\frac{1}{n}} \quad (11)$$

where K_F ($mg^{1-1/n}$ $L^{1/n}$ g^{-1}) is roughly an indicator of the adsorption capacity and n of the adsorption intensity. Values of $n > 1$ indicate favorable adsorption conditions. The Freundlich isotherm (Fig. 11, Table 5) was best fitted for both adsorbents with larger determination coefficients ($R^2 \geq 0.974$ for NS and $R^2 \geq 0.965$ for IS) and lower chi-square values ($\chi^2 \leq 0.601$ for NS and $\chi^2 \leq 0.117$ for IS). The R^2 values calculated for the Langmuir isotherm model (Table 5) were in the range of 0.774–0.859 for NS and 0.747–0.806 for IS, indicating that the data fit the Freundlich adsorption equilibrium model better than the Langmuir. The results indicated further that the Ni^{2+} adsorption occurs on a heterogeneous surface by multilayer coverage. The calculated values of the Freundlich adsorption isotherm constant n were >1, which also led to the conclusion that the adsorption processes were favorable.

The Ni^{2+} adsorption capacities of the two sepiolite samples (Table 6) revealed that differences are due to the properties of each adsorbent, such as structure, functional groups, and surface area. The experimental data for the present study are comparable to other reported values (Yavuz et al. 2003; Alemayehu and Lennartz 2010; Sheikhhosseini et al. 2014). Although both of the adsorbents studied have large adsorption capacities, the NS sample was greater because of its greater BET surface area, porosity, and sepiolite content.

Thermodynamic Parameters

The determination of thermodynamic parameters is of great importance in evaluating the spontaneity and the heat change of the adsorption processes. Changes in Gibbs free energy ($\Delta G°$), enthalpy ($\Delta H°$), and entropy ($\Delta S°$) were determined to estimate the effect of temperature on Ni^{2+} adsorption onto NS and IS. The relationship between the adsorption equilibrium constant and temperature is given by the van't Hoff equation:

$$\ln K_d = \frac{-\Delta G°}{RT} = \frac{\Delta S°}{R} - \frac{\Delta H°}{RT} \quad (12)$$

and, if total activity coefficients for the solute and solvent cancel or equal unity,

$$K_d = \frac{q_e}{C_e} \quad (13)$$

where K_d (L g^{-1}) is the thermodynamic equilibrium constant, q_e (mg g^{-1}) is the amount of Ni^{2+} adsorbed at equilibrium, and C_e (mg L^{-1}) is the equilibrium concentration of Ni^{2+} in solution. R and T are the universal gas constant (8.314 J mol^{-1} K^{-1}) and the absolute solution temperature (K), respectively. The values of $\Delta S°$ and $\Delta H°$ were calculated from the intercept and the slope of the linear plot of $\ln K_d$ vs $1/T$ (Fig. 12), respectively. From the values of $\Delta H°$ and $\Delta S°$, $\Delta G°$ can be calculated using the relation below:

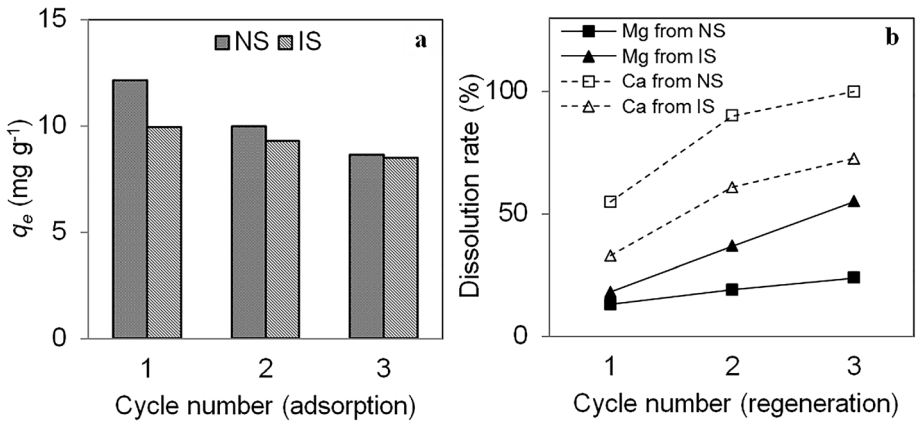

Fig. 13. a Reusability of NS and IS for Ni^{2+} adsorption, **b** extent of dissolution of Mg and Ca during regeneration

https://doi.org/10.1007/s42860-020-00077-7 Published online by Cambridge University Press

Table 8. Cost estimation for the adsorbents used in this study

Components	Cost break-down	Estimated costs (USD kg^{-1} adsorbent)	
		NS	IS
Cost of raw material	NS was supplied free of charge as carving residue; the cost of IS (not charged in this case) was that given by the supplier, Sakarya Minerals Ind. Trade Co. Ltd., Eskişehir.	0	0.044
Cost of transportation	Based on the vehicle rental prices	0.10	0.10
Cost of drying	Hour×unit×unit cost (3×0.2×0.15)	0.09	0.09
Cost of size reduction	Electricity consumption×unit cost (0.1×0.15)	0.015	0.015
Net cost	–	0.21	0.25
Overhead charge	10% of overall cost	0.02	0.02
Total cost	–	0.23	0.27

$$\Delta G^\circ = \Delta H^\circ - T\Delta S^\circ \quad (14)$$

The negative values of ΔG° (between –5.70 and –11.92 kJ mol^{-1} for NS; –5.24 and –11.93 kJ mol^{-1} for IS) at all the temperatures indicated that Ni^{2+} adsorption was spontaneous and thermodynamically feasible (Table 7). The greater negative values for ΔG° with increasing temperature indicated that the extent of the adsorption reaction increased with higher temperatures. Values for ΔG° for physical adsorption are usually between 0 and –20 kJ mol^{-1}, whereas for chemical adsorption they are often in the range of –80 to –400 kJ mol^{-1} (Özcan et al. 2007), indicating that physical adsorption was the probable mechanism for Ni^{2+} removal by NS and IS . The positive ΔH° values (86.77 kJ mol^{-1} for NS) and (94.51 kJ mol^{-1} for IS) showed that the adsorption of Ni^{2+} onto these minerals was endothermic, so an increase in entropy had to be the driving force in order to obtain the spontaneous condition $\Delta G^\circ < 0$. The entropy changes were 334.41 J mol^{-1} K^{-1} for IS and 309.81 J mol^{-1} K^{-1} for NS, which values exceeded those for ΔH° and thus satisfied the spontaneous condition. The positive values for ΔS° indicated a decrease in the order of the system, probably because Ni^{2+} ions were less hydrated on the clay surfaces than in the aqueous solution (Sheikhhosseini et al. 2014).

Reusability Studies

Regeneration and reuse of adsorbent is an important matter in adsorption studies as it increases the economic value of the adsorption process. Estimating the regeneration ability of an adsorbent after it has been used for adsorption is, therefore, necessary. For this purpose, a 0.1 M HCl solution was used to elute Ni^{2+} adsorbed on the sepiolite samples. The dissolution rate of sepiolite has been reported to increase with increasing acid concentration (Özdemir and Kıpçak 2004). The dissolution rate of magnesite containing dolomite has also been reported to increase significantly above 0.1 M hydrochloric acid concentration (Özdemir et al. 2009). A more concentrated acid solution was not used, therefore, as a regenerant in the present study. The adsorption capacities of the two adsorbents tended to decrease with increasing number of cycles (Fig. 13a). After the third cycle, however, the NS and IS samples still had relatively large adsorption capacities of 8.63 mg g^{-1} and 8.43 mg g^{-1}, respectively. The acid solution may have counteracted some of the loss in adsorption capacity in subsequent cycles by increasing the surface area, porosity, and active centers of the NS and IS, as noted by Lazarevic et al. (2007). These results suggested that the samples exhibited reusability and could be a potential recyclable adsorbent for the removal of Ni^{2+} ions from aqueous solution.

Table 9. Comparison of estimated cost of adsorbents reported for Ni removal

Adsorbent type	Estimated costs		References
	(USD kg^{-1} adsorbent)	(USD kg^{-1} adsorbate)	
Sludge-derived MnO_2	151.67	1266	Ong et al. (2018)
Magnetite-based nanocomposite	66.5	3239	Baseri and Tizro (2017)
Modified biochar	–	14.57	Mahdi et al. (2019)
Activated carbon	1.22	19.14	Pap et al. (2017)
Ca-Mg phosphate	0.5	21.03	Ivanets et al. (2017)
Biosorbent (*Saccharum bengalense*)	0.052	3.29	Din and Mirza (2013)
NS	0.23	18.93	Present study
IS	0.27	27.11	Present study

https://doi.org/10.1007/s42860-020-00077-7 Published online by Cambridge University Press

To test the stability of the adsorbents further, the Mg and Ca concentrations in the solutions after each regeneration cycle were measured, and the extent of dissolution of these elements with each cycle was calculated (Fig. 13b). The extent of dissolution of Ca (~55–100% for NS and ~33–73% for IS) was greater than of Mg (~13–24% for NS and ~18–55% for IS), showing that the dolomite is readily soluble. The amount of Mg dissolved from NS was less from cycle to cycle (flatter slope) than for IS, indicating that NS was more stable in the acidic regeneration medium.

Cost Estimation

Successful industrial implementation of an adsorptive removal technique for a contaminant depends heavily on the cost of the adsorbent as well as its physicochemical properties. The availability of adsorbent, processing requirements, treatment conditions, and reusability are the main parameters affecting the adsorbent cost. The estimated total costs together with the break-up costs to prepare 1 kg of adsorbent are summarized in Table 8. In addition, the comparisons of the costs of adsorbents used in this study with others reported previously are given in Table 9. The removal costs per kg of adsorbate were calculated using the estimated adsorbent costs and the removal capacities of adsorbents. The costs calculated for NS and IS were comparable with the other reported adsorbents (Baseri and Tizro 2017; Ong et al. 2018). The present study has, therefore, confirmed that NS and IS, as cost-effective and eco-friendly adsorbents, could be used for the treatment of wastewater containing Ni^{2+}.

CONCLUSIONS

This research has demonstrated the potential of nodular sepiolite (NS) and industrial sepiolite (IS) as effective, economic, and environment-friendly adsorbents for the removal of Ni^{2+} ions from aqueous solutions. The adsorbents were characterized by XRD, XRF, BET, SEM/EDS, and FTIR analyses. The XRD and XRF analyses showed that both sepiolite samples contain magnesite and dolomite as impurities, and the proportions of these minerals in IS were greater. The specific surface areas of NS and IS were measured as being 182.19 $m^2\ g^{-1}$ and 63.78 $m^2\ g^{-1}$, respectively. The FTIR analysis suggested that the –OH and Si–O groups contributed to the adsorption of Ni^{2+} ions from the solution. The adsorption behavior of Ni^{2+} on NS and IS was affected by experimental parameters such as adsorbent dosage, pH, contact time, initial concentration of Ni^{2+}, and temperature. The optimum adsorbent dosage was determined as 0.6 g/50 mL and the optimum pH value was 6.0, for both samples. The adsorption process was described well by the pseudo-second order kinetics model (k_2: 0.0049–0.0397 g $mg^{-1}\ min^{-1}$ for NS and 0.0688–0.1195 g $mg^{-1}\ min^{-1}$ for IS) and the Freundlich isotherm model (K_F: 4.89–9.73 $mg^{1-1/n}\ L^{1/n}\ g^{-1}$ for NS and 4.27–6.42 $mg^{1-1/n}\ L^{1/n}\ g^{-1}$ for IS). Adsorption capacities were 12.15 mg g^{-1} and 9.96 mg g^{-1} for NS and IS, respectively, at 25°C, when studied with a 500 mg L^{-1} Ni^{2+} solution. The greater adsorption capacity of NS may be due to the larger surface area and its larger sepiolite content. Feasibility, spontaneity and randomness of the process were determined from the thermodynamic state functions $\Delta G°$, $\Delta H°$, and $\Delta S°$. The adsorption process was spontaneous ($\Delta G°$: –5.70 to –11.92 kJ mol^{-1} for NS and –5.24 to –11.93 kJ mol^{-1} for IS) and endothermic ($\Delta H°$: 86.77 kJ mol^{-1} for NS and 94.51 kJ mol^{-1} for IS), and the randomness increased ($\Delta S°$: 309.81 J $mol^{-1}\ K^{-1}$ for NS and 334.41 J $mol^{-1}\ K^{-1}$ for IS). These results suggested a physical adsorption mechanism on a heterogeneous surface by multilayer coverage. Results revealed that reuse of NS and IS for Ni^{2+} removal is feasible over multiple adsorption cycles. The stability of the adsorbents was monitored by measuring the extent of dissolution of Mg and Ca in the samples during regeneration, and the NS was found to be more stable in the acidic regenerant medium. The cost-effectiveness of the adsorbents was confirmed by a comprehensive cost analysis. The cost to remove 1 kg of adsorbate was calculated as 18.93 USD for NS and 27.11 USD for IS. As a result, both NS and IS would be useful for the economic treatment of wastewater containing Ni^{2+} because of their quite low costs.

Compliance with Ethical Standards

Conflict of Interest

The authors declare that they have no conflict of interest.

REFERENCES

Ahribesh, A. A., Lazarevic, S., Jankovic-Castvan, I., Jokic, B., Spasojevic, V., Radetic, T., Janackovic, D., & Petrovic, R. (2017). Influence of the synthesis parameters on the properties of the sepiolite-based magnetic adsorbents. *Powder Technology, 305*, 260–269.

Alemayehu, E., & Lennartz, B. (2010). Adsorptive removal of nickel from water using volcanic rocks. *Applied Geochemistry, 25*, 1596–1602.

Alkan, M., Tekin, G., & Namli, H. (2005). FTIR and zeta potential measurements of sepiolite treated with some organosilanes. *Microporous and Mesoporous Materials, 84*, 75–83.

Alvani, S., Hojati, S., & Landi, A. (2019). Effects of sepiolite nanoparticles on the kinetics of Pb and Cu removal from aqueous solutions and their immobilization in columns with different soil textures. *Geoderma, 350*, 19–28.

An, Q., Jiang, Y. Q., Nan, H. Y., Yu, Y., & Jiang, J. N. (2019). Unraveling sorption of nickel from aqueous solution by $KMnO_4$ and KOH-modified peanut shell biochar: Implicit mechanism. *Chemosphere, 214*, 846–854.

Argun, M. E., Dursn, S., Gür, K., Özdemir, C., Karataş, M., & Doğan, S. (2005). Nickel adsorption on the modified pine tree materials. *Environmental Technology, 26*, 479–487.

Bahabadi, F. N., Farpoor, M. H., & Mehrizi, M. H. (2017). Removal of Cd, Cu and Zn ions from aqueous solutions using natural and Fe modified sepiolite, zeolite and palygorskite clay minerals. *Water Science and Technology, 75*, 340–349.

Baseri, H., & Tizro, S. (2017). Treatment of nickel ions from contaminated water by magnetite based nanocomposite adsorbents: Effects of thermodynamic and kinetic parameters and modeling with Langmuir and Freundlich isotherms. *Process Safety and Environmental Protection, 109*, 465–477.

https://doi.org/10.1007/s42860-020-00077-7 Published online by Cambridge University Press

Brauner, K., & Preisinger, A. (1956). Struktur und entstehung des sepioliths. *Tschermaks mineralogische und petrographische Mitteilungen, 6*, 120–140.

Carvalho, W. A., Vignado, C., & Fontana, J. (2008). Ni(II) removal from aqueous effluents by silylated clays. *Journal of Hazardous Materials, 153*, 1240–1247.

Cempel, M., & Nikel, G. (2006). Nickel: A review of its sources and environmental toxicology. *Polish Journal of Environmental Studies, 15*, 375–382.

Crini, G., & Badot, P. M. (2010). *Sorption Process and Pollution, Conventional and Non-Conventional Sorbents for Pollutant Removal from. Wastewaters*: Presses Universitaires de Franche-Comté.

Dabiri, R., & Shiraz, E. A. (2018). Evaluating performance of natural sepiolite and zeolite nanoparticles for nickel, antimony, and arsenic removal from synthetic wastewater. *Journal of Mining and Environment, 9*, 1049–1064.

Din, M. I., & Mirza, M. L. (2013). Biosorption potentials of a novel green biosorbent Saccharum bengalense containing cellulose as carbohydrate polymer for removal of Ni (II) ions from aqueous solutions. *International Journal of Biological Macromolecules, 54*, 99–108.

Duman, O., Tunç, S., & Polat, T. G. (2015). Adsorptive removal of triarylmethane dye (Basic Red 9) from aqueous solution by sepiolite as effective and low-cost adsorbent. *Microporous and Mesoporous Materials, 210*, 176–184.

Eren, E., & Gumus, H. (2011). Characterization of the structural properties and Pb(II) adsorption behavior of iron oxide coated sepiolite. *Desalination, 273*, 276–284.

Eren, E., Gumus, H., & Ozbay, N. (2010). Equilibrium and thermodynamic studies of Cu(II) removal by iron oxide modified sepiolite. *Desalination, 262*, 43–49.

Fersman, A. E. (1913). Research on magnesium silicates. *Zapiski Imperatorskoi Akademii Nauk, 32*, 321–430.

Franco, F., Pozo, M., Cecilia, J. A., Benítez-Guerrero, M., Pozo, E., & Martín Rubí, J. A. (2014). Microwave assisted acid treatment of sepiolite: The role of composition and "crystallinity". *Applied Clay Science, 102*, 15–27.

Freundlich, H. (1926). *Colloid and Capillary Chemistry*. London: Methuen.

Frost, R. L., Locos, O. B., Ruan, H., & Kloprogge, J. T. (2001). Near-infrared and mid-infrared spectroscopic study of sepiolites and paligorskites. *Vibrational Spectroscopy, 27*, 1–13.

Glatstein, D. A., & Francisca, F. M. (2015). Influence of pH and ionic strength on Cd, Cu and Pb removal from water by adsorption in Na-bentonite. *Applied Clay Science, 118*, 61–67.

Gregg, S. J., & Sing, K. S. W. (1982). *Adsorption, Surface Area and Porosity* (2nd ed.). London: Academic Press.

Guerra, D. L., Batista, A. C., Correa da Costa, P. C., Viana, R. R., & Airoldi, C. (2010). Adsorption of arsenic ions on Brazilian sepiolite: Effect of contact time, pH, concentration, and calorimetric investigation. *Journal of Colloid and Interface Science, 346*, 178–187.

Gulensoy, H. (1984). *Kompleksometrik Titrasyonlar ve Kompleksometrinin Temelleri*. Istanbul: Fatih Press.

Guo, N., Wang, J. S., Li, J., Teng, Y. G., & Zhai, Y. Z. (2014). Dynamic adsorption of Cd^{2+} onto acid-modified attapulgite from aqueous solution. *Clays and Clay Minerals, 62*, 415–424.

Gupta, S. S., & Bhattacharyya, K. G. (2006). Adsorption of Ni(II) on clays. *Journal of Colloid and Interface Science, 295*, 21–32.

Ho, Y. S., & McKay, G. (1998). Sorption of dye from aqueous solution by peat. *Chemical Engineering Journal, 70*, 115–124.

Ivanets, A. I., Srivastava, V., Kitikova, N. V., Shashkova, I. L., & Sillanpaa, M. (2017). Kinetic and thermodynamic studies of the Co(II) and Ni(II) ions removal from aqueous solutions by Ca-Mg phosphates. *Chemosphere, 171*, 348–354.

Katsou, E., Malamis, S., Haralambous, K. J., & Loizidou, M. (2010). Use of ultrafiltration membranes and aluminosilicate minerals for nickel removal from industrial wastewater. *Journal of Membrane Science, 360*, 234–249.

Kıpçak, İ., & Isıyel, T. G. (2015). Magnesite tailing as low-cost adsorbent for the removal of copper (II) ions from aqueous solution. *Korean Journal of Chemical Engineering, 32*, 1634–1641.

Kocaoba, S. (2009). Adsorption of Cd(II), Cr(III) and Mn(II) on natural sepiolite. *Desalination, 244*, 24–30.

Kocaoba, S. (2020). Adsorption of Fe(II) and Fe(III) from aqueous solution by using sepiolite: speciation studies with MINEQL+ computer program. *Separation Science and Technology, 55*, 896–906.

Lagergren, S. (1898). Zur theorie der sogenannten adsorption gelöster stoffe, kungliga svenska vetenskaps akademiens. *Handlingar, 24*(*4*), 1–39.

Langmuir, I. (1918). The adsorption of gases on plane surfaces of glass, mica and platinum. *Journal of the American Chemical Society, 40*, 1361–1403.

Lata, H., Garg, V. K., & Gupta, R. K. (2008). Sequestration of nickel from aqueous solution onto activated carbon prepared from Parthenium hysterophorus L. *Journal of Hazardous Materials, 157*, 503–509.

Lazarevic, S., Jankovic-Castvan, I., Jovanovic, D., Milonjic, S., Janackovic, D., & Petrovic, R. (2007). Adsorption of Pb^{2+}, Cd^{2+} and Sr^{2+} ions onto natural and acid-activated sepiolites. *Applied Clay Science, 37*, 47–57.

Lazarevic, S., Jankovic-Castvan, I., Djokic, V., Radovanovic, Z., Janackovic, D., & Petrovic, R. (2010). Iron-modified sepiolite for Ni^{2+} sorption from aqueous solution: An equilibrium, kinetic, and thermodynamic study. *Journal of Chemical & Engineering Data, 55*, 5681–5689.

Lescano, L., Castillo, L., Marfil, S., Barbosa, S., & Maiza, P. (2014). Alternative methodologies for sepiolite defibering. *Applied Clay Science, 95*, 378–382.

Lin, S., Zhou, T., & Yin, S. (2017). Properties of thermally treated granular montmorillonite-palygorskite adsorbent (GMPA) and use to remove Pb^{2+} and Cu^{2+} from aqueous solutions. *Clays and Clay Minerals, 65*, 184–192.

Mahdi, Z., El Hanandeh, A., & Yu, Q. J. (2019). Preparation, characterization and application of surface modified biochar from date seed for improved lead, copper, and nickel removal from aqueous solutions. *Journal of Environmental Chemical Engineering, 7*, 103379.

Malkoç, E., & Nuhoğlu, Y. (2005). Investigations of nickel(II) removal from aqueous solutions using tea factory waste. *Journal of Hazardous Materials, B127*, 120–128.

Malkoç, E., & Nuhoğlu, Y. (2006). Removal of Ni(II) ions from aqueous solutions using waste of tea factory: Adsorption on a fixed-bed column. *Journal of Hazardous Materials, B135*, 328–336.

Milicevic, S., Milosevic, V., Povrenovic, D., Stojanovic, J., Martinovic, S., & Babic, B. (2013). Removal of heavy metals from aqueous solution using natural and Fe(III) oxyhydroxide clinoptilolite. *Clays and Clay Minerals, 61*, 508–516.

Ong, D. C., Pingul-Ong, S. M. B., Kan, C. C., & de Luna, M. D. G. (2018). Removal of nickel ions from aqueous solutions by manganese dioxide derived from groundwater treatment sludge. *Journal of Cleaner Production, 190*, 443–451.

Özcan, A., Ömeroğlu, Ç., Erdoğan, Y., & Özcan, A. S. (2007). Modification of bentonite with a cationic surfactant: an adsorption study of textile dye Reactive Blue 19. *Journal of Hazardous Materials, 140*, 173–179.

Özdemir, M., & Kıpçak, İ. (2004). Dissolution kinetics of sepiolite in hydrochloric acid and nitric acid. *Clays and Clay Minerals, 52*, 714–720.

Özdemir, M., Çakır, D., & Kıpçak, İ. (2009). Magnesium recovery from magnesite tailings by acid leaching and production of magnesium chloride hexahydrate from leaching solution by evaporation. *International Journal of Mineral Processing, 93*, 209–212.

Pap, S., Knudsen, T. S., Radonic, J., Maletic, S., Igic, S. M., & Sekulic, M. T. (2017). Utilization of fruit processing industry waste as green activated carbon for the treatment of heavy metals and chlorophenols contaminated water. *Journal of Cleaner Production, 162*, 958–972.

Pehlivan, E., & Arslan, G. (2007). Removal of metal ions using lignite in aqueous solution-Low cost biosorbents. *Fuel Processing Technology, 88*, 99–106.

Qiu, Y., Yu, S., Song, Y., Wang, Q., Zhong, S., & Tian, W. (2013). Investigation of solution chemistry effects on sorption behavior of Sr(II) on sepiolite fibers. *Journal of Molecular Liquids, 180*, 244–251.

Raval, N. P., Shah, P. U., & Shah, N. K. (2016). Adsorptive removal of nickel(II) ions from aqueous environment: A review. *Journal of Environmental Management, 179*, 1–20.

Sabah, E., & Ouki, S. (2017). Sepiolite and sepiolite-bound humic acid interactions in alkaline media and the mechanism of the formation of sepiolite-humic acid complexes. *International Journal of Mineral Processing, 162*, 69–80.

Sheikhhosseini, A., Shirvani, M., Shariatmadari, H., Zvomuya, F., & Najafic, B. (2014). Kinetics and thermodynamics of nickel sorption to calcium–palygorskite and calcium–sepiolite: A batch study. *Geoderma, 217–218*, 111–117.

Srivastava, N. K., & Majumder, C. B. (2008). Novel biofiltration methods for the treatment of heavy metals from industrial wastewater. *Journal of Hazardous Materials, 151*, 1–8.

Suarez, M., & Garcia-Romero, E. (2012). Variability of the surface properties of sepiolite. *Applied Clay Science, 67–68*, 72–82.

Suarez, M., Garcia-Rivas, J., Garcia-Romero, E., & Jara, N. (2016). Mineralogical characterisation and surface properties of sepiolite from Polatlı (Turkey). *Applied Clay Science, 131*, 124–130.

Uddin, M. K. (2017). A review on the adsorption of heavy metals by clay minerals, with special focus on the past decade. *Chemical Engineering Journal, 308*, 438–462.

Weber, W. J., & Morris, J. C. (1963). Kinetics of adsorption on carbon from solution. *Journal of the Sanitary Engineering Division, ASCE, 89*, 31–60.

WHO. (2011). *Guidelines for Drinking-Water Quality* (4th ed.). Switzerland: World Health Organization.

Wu, X., Zhang, Q., Liu, C., Zhang, X., & Chung, D. D. L. (2017). Carbon-coated sepiolite clay fibers with acid pre-treatment as low cost organic adsorbents. *Carbon, 123*, 259–272.

Xu, Z., Jiang, H., Yu, Y., Xu, J., Liang, J., Zhou, L., & Hu, F. (2017). Activation and β-FeOOH modification of sepiolite in one-step hydrothermal reaction and its simulated solar light catalytic reduction of Cr(VI). *Applied Clay Science, 135*, 547–553.

Yavuz, Ö., Altunkaynak, Y., & Güzel, F. (2003). Removal of copper, nickel, cobalt and manganese from aqueous solution by kaolinite. *Water Research, 37*, 948–952.

Yebra-Rodriguez, A., Martin-Ramos, J. D., Del Rey, F., Viseras, C., & Lopez-Galindo, A. (2003). Effect of acid treatment on the structure of sepiolite. *Clay Minerals, 38*, 353–360.

Yeniyol, M. (2014). Characterization of two forms of sepiolite and related Mg-rich clay minerals from Yenidoğan (Sivrihisar, Turkey). *Clay Minerals, 4*, 91–108.

Zhao, J., & He, M. C. (2014). Theoretical study of heavy metal Cd, Cu, Hg, and Ni(II) adsorption on the kaolinite (001) surface. *Applied Surface Science, 317*, 718–723.

(Received 19 July 2019; revised 15 April 2020; AE: Runliang Zhu)